Sensorless Optimal Interaction Control Exploiting Environment Stiffness Estimation

Loris Roveda[1,*], Asad Ali Shahid[2], Niccolò Iannacci[3] and Dario Piga[1]

***Abstract*—Industrial robots are increasingly used to perform tasks that require an interaction with the surrounding environment (*e.g.*, assembly tasks). Such environments are usually (partially) unknown to the robot (in terms of dynamic characteristics), demanding the implemented controllers to suitably react to the established interaction. Standard controllers require force/torque measurements to close the loop, making it, if possible, to adapt the robot behavior to the specific environment. However, most of the industrial manipulators do not have embedded force/torque sensor(s), which entails additional effort in terms of costs and implementation for their integration in the robotic setup. To extend the use of sensorless compliant controllers to force control, a robot-environment interaction dynamics model-based methodology is presented in this paper. Relying on the sensorless Cartesian impedance control, an Extended Kalman Filter (EKF) is proposed to estimate the stiffness of an interaction environment. Exploiting the provided estimation, the robot-environment coupled dynamic modeling is used to design an optimal LQR interaction controller to close the force loop. The control gains can be analytically computed by solving the related Riccati equation, as such gains are a function of the impedance control and environment parameters. In addition, the interaction force can be estimated to close the force loop, making the sensorless robot able to perform the target interaction task. The described approach has been validated with experiments by analyzing two scenarios: a probing task, and a closing of a plastic (*i.e.*, compliant) box with snap-fit closure mechanism. The performance of the proposed control framework have been evaluated, highlighting the capabilities of the EKF and the optimal LQR interaction controller. Finally, the proposed control schema is enhanced by the adaptation of the EKF for the estimation of the external wrench. Two additional experiments are provided to show the improvements on the control schema (a polishing-like task and an assembly task). A Franka EMIKA panda robot has been used as the reference robotic platform for the experimental validation.**

I. Introduction

A. Context

Robots are increasingly involved in daily life activities, providing assistance in many domains [1]. Manipulators are no longer used to execute a simple repetitive task thousands of times, but rather they have to face thousands of different tasks in an ever-changing environment. It will be, therefore, difficult to pre-program all the possible tasks and scenarios, requiring the robot to learn or adapt its behavior on the basis of the operating conditions [2]. Considering the manufacturing context, robots have to provide a flexible solution and adapt to the new tasks/production, while guaranteeing the target performance [3]. Considering interaction tasks (*i.e.*, robot exchanging forces/torques with an environment), the capability to adapt to new scenarios becomes even more critical [4]. To avoid any unwanted or unstable behavior, the interaction force has to be controlled [5]. Common interaction control strategies, however, make use of expensive sensors [6], increasing the hardware costs and the setup time. Many works are investigating external wrench estimation algorithms and control methodologies to close the interaction control loop based on the provided estimations. In this way, it is possible to avoid the use of such costly devices and allow the robot to adapt to uncertain interaction.

B. Related work

Being able to achieve a stable interaction between a sensorless industrial robot and its environment has received a lot of attention from the research community. Two main research fields can be identified: (i) sensorless methodologies for the estimation of the external interaction, and (ii) sensorless control methodologies for the control of the interaction. Considering (i), developed methodologies that rely on robot dynamic identification [7] have been addressed, aiming to derive an accurate robot's dynamical model. [8] proposes a nonlinear disturbance observer to estimate the external interaction. In [9], the filtered dynamic equations are combined with a recursive least-square estimation algorithm to provide a smooth external force estimation. [10] derives a task-oriented dynamics model learning and a robust disturbance state observer to estimate the external interaction. In [11], a convex optimization problem is solved in real time to estimate the interaction force accounting for velocity-dependent uncertainties of the Coulomb friction. A parametric robot dynamic model based on rigid-body dynamic is combined with a non-parametric model to compensate for uncertainties in the work investigated in [12]. A disturbance Kalman filter is then developed to perform the interaction force estimation. [13] describes the implementation of a virtual force sensor to estimate the interaction force by exploiting the task-oriented robot dynamic model calibration. This dynamic model is then used to estimate the external joint torques as the difference between measured motor torques and modelled torques (*i.e.*, residual method). In addition to the works described above, external sensors have also been used in order to improve the accuracy of the external force estimation. [14] detects external contacts between the robot and the environment using a depth camera, while simultaneously determining the external joint torques using the residual method.

[1] Loris Roveda and Dario Piga are with Istituto Dalle Molle di studi sull'Intelligenza Artificiale (IDSIA), Scuola Universitaria Professionale della Svizzera Italiana (SUPSI), Università della Svizzera italiana (USI), via Cantonale 2C- 6928, Manno, Switzerland loris.roveda@idsia.ch, dario.piga@idsia.ch

[2] Asad Ali Shahid is with Politecnico di Milano, Department of Mechanical Engineering, Milano, Italy asadali.shahid@mail.polimi.it

[3] niccolo.iannacci@gmail.com

The work has been developed within the project ASSASSINN, funded from H2020 CleanSky 2 under grant agreement n. 886977.

Other methodologies have been developed in order to map the interaction between the robot and the environment, exploiting such learned dynamics in the controller. [15] employs a position loop to control the interaction by exploiting the external force estimation between the robotic tool and a soft tissue. [16] has developed a Neural Networks approach to map the interaction forces between the robot and a soft environment by exploiting the motor current measurements. [17] implements a sensorless admittance control scheme by exploiting a disturbance observer to model the linear environment dynamics together with a radial basis Neural Networks approach to compensate for modeling uncertainties. In [18], the derivation of a Neural Network approach to classify force ranges from optical coherence tomography (OCT) images is described. [19] details a force estimation model based on Convolutional Neural Networks and Long-Short Term Memory networks. In [20], an online sparse Gaussian process regression (OSGPR) approach is used to estimate the interaction forces between the slave manipulator and its surrounding environment for a bilateral tele-operation system.

Considering (ii), methodologies to control the interaction by exploiting the provided estimations have been proposed. [21] defines a control law based on Lyapunov techniques to track a target force without its measurements. In [22], a nonlinear matrix mapping function between each joint motor control input and the end-effector actuation force/torques vector is achieved. Such a mapping is used into a model-free fuzzy sliding mode control for interaction control. [23] designs an admittance control to perform an insertion task. A real-time trajectory generator is proposed to perform the assembly by exploiting the model-based sensorless observer of the interaction forces. A force/position decentralized robust control problem for constrained reconfigurable manipulator system with parameter perturbation and unmodeled dynamics is presented in [24]. [25] investigates a force estimation approach based on a dither periodic component elimination Kalman filter and on a disturbance observer for realization of a fine sensorless force control system under the existence of static friction. [26] makes use of a notch-type friction free disturbance observer for sensorless force control purposes.

Addressing model-based approaches, state of the art methods allow to estimate and control the interaction between the robot and the environment by only making use of the robot's dynamical model, without modeling and estimating the environment dynamics. Such modeling and estimation, however, is of great importance to design the interaction controller to avoid instabilities and to achieve the required performance [27], [28]. To the authors' knowledge, the only sensorless approach estimating the environment compliance can be found in [29]. An adaptive force/position controller is proposed by exploiting a position-based force estimator and a force-based environment compliance estimator. However, the convergence of this method is guaranteed only in the presence of a persistent (*i.e.*, dynamic) excitation (*i.e.*, a constant reference force cannot be applied - as required by many industrial tasks). Therefore, the present paper aims to extend the sensorless force control literature by designing an environment stiffness observer to be exploited by the controller. In particular, the proposed sensorless LQR interaction controller allows to tune the control gains on the basis of provided estimation, while using the estimation of the interaction force to close the force loop.

C. Paper Contribution

Extending the work in [30] and relying on sensorless Cartesian impedance control, the proposed contribution aims to design a sensorless model-based methodology to enhance interaction control without the use of force/torque sensors on industrial manipulators. To this end, an Extended Kalman Filter (EKF) is designed to estimate the stiffness of an interaction environment, so that the coupled robot-environment dynamic model can be defined. The EKF takes into account the non-linear coupled robot dynamics resulting from the sensorless Cartesian impedance controller, together with the environment dynamics. By exploiting such an estimation, the coupling terms in the controlled robot dynamics can be compensated. In this way, it is possible to design an optimal LQR interaction controller by using the dynamic modeling of the robot-environment. The control gains can be analytically computed as a function of the environment stiffness parameter, and updated online on the basis of the provided estimation. The interaction force can then be estimated in order to close the force loop, making use of the estimated environment stiffness. W.r.t. the environment stiffness estimation, the main advantage of the proposed approach is that no persistent (*i.e.*, dynamic) excitation is required to perform the estimation [29]. In fact, the equivalent elastic force of the environment is only proportional to the penetration of the robot into the environment, and it is possible to extract such an information from the difference between the robot's Cartesian position and the estimated equilibrium position of the environment. Considering the proposed optimal LQR interaction controller, the main advantage of the proposed approach is that the control gains can be computed online by exploiting the environment stiffness estimation, guaranteeing stability and the optimal control action computation. The described approach has been validated with experiments, employing a Franka EMIKA panda robot. Two tasks have been implemented: a probing task (with two different unknown environments in interaction with a robot, a soft environment and a stiff environment), and the closing of a plastic (*i.e.*, compliant) box. W.r.t. the second task, the plastic box has a snap-fit closure mechanism, *i.e.*, a compliant closure system that requires to overcome a reference force for its proper closing. Experimental results show the capabilities of both the EKF (for the estimation of the environment stiffness and interaction force), and of the optimal LQR interaction controller (for force tracking capabilities). The proposed control schema is finally enhanced employing the estimation of the external wrench by adapting the proposed EKF for this purpose. The derived EKF modification allows to directly estimate the interaction between the robot and the environment, detecting no contact/contact transitions to enable the environment stiffness estimation as needed. Two tasks have been considered for the validation of the improved controller: a polishing-like task and an assembly task. Experimental results show the achieved control performance.

D. Paper outline

The paper is structured as follows. Section II introduces the proposed control schema. Section III describes the implemented inner sensorless Cartesian impedance controller with redundancy management. In Section IV, the derivation of the Extended Kalman Filter for estimating the (unknown) environment stiffness is presented. Section V proposes the design of the outer interaction controller, including both the coupling compensator and the optimal LQR interaction controller exploiting estimations from the EKF. Section VI provides the experimental results for both the EKF and the optimal LQR interaction controller. Section VII adapts the proposed EKF for the estimation of the external wrench, providing additional experimental results related to the improved control schema. Conclusions and directions for future work are given in Section VIII.

II. Controller Definition

The presented paper describes a methodology to control the interaction between a (partially) unknown environment and a sensorless robot, making it possible to track a reference interaction force. In order to develop this sensorless interaction controller, the following components defining the control schema are proposed: (i) a sensorless Cartesian impedance controller, (ii) an inner Extended Kalman Filter (EKF), (iii) an outer coupling compensator, and (iv) an outer optimal LQR interaction controller. (i) aims to implement a compliant behavior for the controlled manipulator without the use of force/torque measurements, in order to achieve a safe and stable interaction with the (partially) unknown target environment, even for a sensorless robot. (ii) estimates the interaction environment stiffness, to be used for the estimation of the interaction force and by the controller for the tuning of its gains. (iii) is designed to deal with the coupled controlled dynamics resulting from the inner sensorless Cartesian impedance controller. (iv) is the outer optimal LQR interaction controller. Exploiting the estimation of the environment stiffness provided by the EKF, the control gains are computed and updated at each control step (to track any change in the environment stiffness, *e.g.*, for non-linear environments) to compute the optimal control action. The control actions provided by (iii) and (iv) are used to update the setpoint for the inner sensorless Cartesian impedance control, hence, achieving the tracking of reference interaction force. The proposed control schema is shown in Figure **??**.

III. Inner compliant robot control

The sensorless Cartesian impedance control has to be implemented in order to achieve a compliant behavior of the robot without the use of any force/torque measurement. In fact, the control law described below does not make use of measured or estimated force/torque signals that are included in the sensor-based implementation of the Cartesian impedance control. As it will be underlined deriving the controlled robot dynamics, such implementation results in a coupling between the robot's Cartesian degrees of freedom (DoFs), that represents the main difference between the sensorless and sensor-based Cartesian impedance control implementation (in which the DoFs coupling is not present). To linearize the controlled robot dynamics, such coupling will be compensated by the outer control loop. In addition, the implemented inner sensorless Cartesian impedance controller will then be exploited to design the optimal LQR interaction controller.

A. Inner sensorless Cartesian impedance control

To design the proposed sensorless Extended Kalman Filter for the estimation of the interaction environment stiffness, the sensorless Cartesian impedance controller has to be implemented on the robot. The following manipulator dynamics is considered [31]:

$$\mathbf{B}(\mathbf{q})\ddot{\mathbf{q}}+\mathbf{C}(\mathbf{q},\dot{\mathbf{q}})+\mathbf{g}(\mathbf{q})+\boldsymbol{\tau}_f(\mathbf{q},\dot{\mathbf{q}})=\boldsymbol{\tau}-\mathbf{J}(\mathbf{q})^T\mathbf{h}_{ext}, \quad (1)$$

where $\mathbf{B}(\mathbf{q})$ represents the inertia matrix, $\mathbf{C}(\mathbf{q},\dot{\mathbf{q}})$, the Coriolis vector, $\mathbf{g}(\mathbf{q})$, the gravitational vector, $\boldsymbol{\tau}_f(\mathbf{q},\dot{\mathbf{q}})$, the robot joint friction vector, and $\mathbf{q}$, the joint position vector. The Jacobian matrix is denoted by $\mathbf{J}(\mathbf{q})$, whereas $\boldsymbol{\tau}$ and $\mathbf{h}_{ext}$ are the robot joint torque vector and the external force/torque vector.
Based on (1), it is possible to design the sensorless Cartesian impedance controller with dynamics compensation as described in [31], defining the robot joint torque vector $\boldsymbol{\tau}$ as:

$$\boldsymbol{\tau}=\mathbf{B}(\mathbf{q})\boldsymbol{\gamma}+\mathbf{C}(\mathbf{q},\dot{\mathbf{q}})+\mathbf{g}(\mathbf{q})+\boldsymbol{\tau}_f(\mathbf{q},\dot{\mathbf{q}}), \quad (2)$$

where $\boldsymbol{\gamma}$ is the sensorless Cartesian impedance control law. $\boldsymbol{\gamma}$ indicates the reference acceleration to be given to the robot to implement a mass-spring-damper controlled behavior without the exploitation of any force/torque measurement. Therefore, $\boldsymbol{\gamma}$ includes the translational $\ddot{\mathbf{p}}$ and rotational $\dot{\boldsymbol{\omega}}_{cd}$ (described by the intrinsic Euler angles representation) acceleration components of the sensorless Cartesian impedance control. $\boldsymbol{\gamma}$ can be written as:

$$\begin{aligned}\ddot{\mathbf{p}}&=\mathbf{M}_t^{-1}\left(-\mathbf{D}_t\dot{\mathbf{p}}-\mathbf{K}_t\Delta\mathbf{p}\right),\\ \dot{\boldsymbol{\omega}}_{cd}&=\mathbf{M}_r^{-1}\left(-\mathbf{D}_r\dot{\boldsymbol{\varphi}}_{cd}-\mathbf{K}_r\boldsymbol{\varphi}_{cd}\right).\end{aligned} \quad (3)$$

Remark 1. It should be noted that (3) does not make use of any force/torque measurement, therefore, the implemented controller is sensorless w.r.t. the interaction wrench.

Taking into account the translational part of the sensorless Cartesian impedance control, $\mathbf{M}_t$ is the mass matrix, $\mathbf{D}_t$, the damping matrix, and $\mathbf{K}_t$, the stiffness matrix. $\mathbf{p}$ denotes the actual Cartesian position vector, while $\Delta\mathbf{p}=\mathbf{p}-\mathbf{p}^d$, where $\mathbf{p}^d$ is the target position vector. Concerning the rotational part of the sensorless Cartesian impedance control, $\mathbf{M}_r$ specifies the inertia matrix, $\mathbf{D}_r$, the damping matrix, and $\mathbf{K}_r$, the stiffness matrix. $\boldsymbol{\varphi}_{cd}$ is the set of Euler angles extracted from $\mathbf{R}_c^d=\mathbf{R}_d^T\mathbf{R}_c$, describing the mutual orientation between the compliant frame $\mathbf{R}_c$ (at the end-effector) and the target frame $\mathbf{R}_d$. It should be noted that, in the proposed implementation, reference velocity and acceleration signals are not implemented for the damping and inertia terms. It is possible, however, to include such terms in the above definition of the sensorless Cartesian impedance control (3).

Angular accelerations $\dot{\boldsymbol{\omega}}_{cd}$ can be computed as follows:

$$\dot{\boldsymbol{\omega}}_{cd}=\mathbf{T}(\boldsymbol{\varphi}_{cd})\left(\mathbf{M}_r^{-1}\left(-\mathbf{D}_r\dot{\boldsymbol{\varphi}}_{cd}-\mathbf{K}_r\boldsymbol{\varphi}_{cd}\right)\right)+\dot{\mathbf{T}}(\boldsymbol{\varphi}_{cd})\dot{\boldsymbol{\varphi}}_{cd}, \quad (4)$$

where matrix $\mathbf{T}(\boldsymbol{\varphi}_{cd})$ defines the transformation from Euler angles derivatives to angular velocities $\boldsymbol{\omega}_{cd} = \mathbf{T}(\boldsymbol{\varphi}_{cd})\dot{\boldsymbol{\varphi}}_{cd}$, and $\boldsymbol{\omega} = \mathbf{R}_{ee}\boldsymbol{\omega}_{cd}$ (with $\mathbf{R}_{ee}$ the rotation matrix from the robot base to its end-effector) [31]. Since the implementation of the proposed controller relies on the selected Euler angles convention, it should be noted that its definition needs to be provided. In the present paper, the Euler ZYX angle convention has been used for the implementation of the proposed sensorless Cartesian impedance control.

By defining $\widetilde{\mathbf{M}}_r = (\mathbf{R}_{ee}\mathbf{T}(\boldsymbol{\varphi}_{cd}))^{-1}\mathbf{M}_r$ and $\widetilde{\mathbf{D}}_r = \mathbf{D}_r - \widetilde{\mathbf{M}}_r\mathbf{R}_{ee}\dot{\mathbf{T}}(\boldsymbol{\varphi}_{cd})$, (4) can be written as:

$$\dot{\boldsymbol{\omega}} = \widetilde{\mathbf{M}}_r^{-1}\left(-\widetilde{\mathbf{D}}_r\dot{\boldsymbol{\varphi}}_{cd} - \mathbf{K}_r\boldsymbol{\varphi}_{cd}\right). \tag{5}$$

The formulation resulting from (5), (4), and (3) can be written in a compact form as follows:

$$\ddot{\mathbf{x}}^{imp} = -\mathbf{M}^{-1}\left(\mathbf{D}\dot{\mathbf{x}} + \mathbf{K}\Delta\mathbf{x}\right), \tag{6}$$

where the target acceleration computed by the sensorless Cartesian impedance control is $\ddot{\mathbf{x}}^{imp} = [\ddot{\mathbf{x}}_t; \ddot{\mathbf{x}}_r] = [\ddot{\mathbf{p}}; \dot{\boldsymbol{\omega}}]$. $\mathbf{M} = [\mathbf{M}_t\,\mathbf{0}; \mathbf{0}\,\widetilde{\mathbf{M}}_r]$, $\mathbf{D} = [\mathbf{D}_t\,\mathbf{0}; \mathbf{0}\,\widetilde{\mathbf{D}}_r]$, $\mathbf{K} = [\mathbf{K}_t\,\mathbf{0}; \mathbf{0}\,\mathbf{K}_r]$ are the sensorless Cartesian impedance mass, damping and stiffness matrices composed by both the translational and rotational parts, and $\Delta\mathbf{x} = \mathbf{x} - \mathbf{x}^d = [\Delta\mathbf{p}; \boldsymbol{\varphi}_{cd}]$. $\mathbf{x}$ is the current pose vector of the robot's end-effector with both translational and rotational components, while $\mathbf{x}^d$ indicates the reference pose vector of the robot's end-effector with both translational and rotational components. The sensorless Cartesian impedance control law $\boldsymbol{\gamma}$ can then be written as follows:

$$\boldsymbol{\gamma} = \mathbf{J}(\mathbf{q})^{-1}\left(\ddot{\mathbf{x}}^{imp} - \dot{\mathbf{J}}(\mathbf{q},\dot{\mathbf{q}})\dot{\mathbf{q}}\right). \tag{7}$$

For the redundant manipulators, the matrix $\mathbf{J}(\mathbf{q})^{-1}$ can be substituted with the pseudo-inverse of the Jacobian matrix, $\mathbf{J}(\mathbf{q})^{\#}$ [32], with an appropriate choice of the null-space behavior.

Substituting (2) in (1), under the hypothesis that the manipulator dynamics is known (such identification can be performed with the state-of-the-art techniques [33]), the controlled robot dynamics results in:

$$\ddot{\mathbf{q}} = \boldsymbol{\gamma} - \mathbf{B}(\mathbf{q})^{-1}\mathbf{J}(\mathbf{q})^T\mathbf{h}_{ext}, \tag{8}$$

where $\mathbf{h}_{ext} = [\mathbf{f}, \mathbf{T}^T(\boldsymbol{\varphi}_{cd})\boldsymbol{\mu}^d]$ (considering the external forces $\mathbf{f}$ and the external torques $\boldsymbol{\mu}^d$ - referred to the target frame $\mathbf{R}_d$ - acting on the robot related to the interaction with the surrounding environment). Substitution of (7) into (8) leads to:

$$\mathbf{J}(\mathbf{q})\ddot{\mathbf{q}} + \dot{\mathbf{J}}(\mathbf{q},\dot{\mathbf{q}})\dot{\mathbf{q}} = \ddot{\mathbf{x}} = \ddot{\mathbf{x}}^{imp} - \mathbf{J}(\mathbf{q})\mathbf{B}(\mathbf{q})^{-1}\mathbf{J}(\mathbf{q})^T\mathbf{h}_{ext}, \tag{9}$$

where $\ddot{\mathbf{x}} = \mathbf{J}(\mathbf{q})\ddot{\mathbf{q}} + \dot{\mathbf{J}}(\mathbf{q},\dot{\mathbf{q}})\dot{\mathbf{q}}$ represents the Cartesian acceleration of the robot's end-effector resulting from the implementation of the proposed sensorless Cartesian impedance controller. Finally, substituting (6) into (9), the controlled robot dynamics resulting from the design of the sensorless Cartesian impedance control is described by the following equation:

$$\mathbf{M}\ddot{\mathbf{x}} + \mathbf{D}\dot{\mathbf{x}} + \mathbf{K}\Delta\mathbf{x} = -\overline{\mathbf{L}}(\mathbf{q})\mathbf{h}_{ext}, \tag{10}$$

where $\overline{\mathbf{L}}(\mathbf{q}) = \mathbf{M}\mathbf{J}(\mathbf{q})\mathbf{B}(\mathbf{q})^{-1}\mathbf{J}(\mathbf{q})^T$.

The resulting dynamic equation is therefore coupled in the Cartesian DoFs by the matrix $\overline{\mathbf{L}}(\mathbf{q})$.

Remark 2. The sensorless Cartesian impedance control, therefore, results in a coupled controlled robot dynamics. Matrix $\overline{\mathbf{L}}(\mathbf{q})$ redistributes interaction forces along all the Cartesian DoFs. While the decoupled robot behavior cannot be achieved by implementing such controller, the sensorless Cartesian impedance control strategy allows to implement a tuneable compliant behavior of the robot, ensuring a safe and stable interaction with the target environment.

Remark 3. It should be noted that the robot dynamics compensation in (2) is based on estimated (*i.e.*, identified) quantities, therefore, resulting in imperfect compensation in real applications.

B. Redundancy management

The Franka EMIKA panda manipulator has been used as a test platform. This robot is redundant and requires managing its null-space configuration while performing the main task. In this paper, a pure damping behavior is proposed for the null-space configuration control, aiming to damp the null-space motion:

$$\boldsymbol{\tau}_R = \mathbf{B}(\mathbf{q})\left(\left(\mathbf{I} - \mathbf{J}(\mathbf{q})^{\#}\mathbf{J}(\mathbf{q})\right)\left(-\mathbf{D}_n\dot{\mathbf{q}}\right)\right), \tag{11}$$

where $\boldsymbol{\tau}_R$ denotes the null-space control torque, $\mathbf{I}$, the identity matrix, $\mathbf{J}(\mathbf{q})^{\#}$, the pseudo-inverse of the Jacobian matrix, and $\mathbf{D}_n$, the null-space damping diagonal matrix. The term $\left(\mathbf{I} - \mathbf{J}(\mathbf{q})^{\#}\mathbf{J}(\mathbf{q})\right)$ is the null-space projection matrix. The term $-\mathbf{D}_n\dot{\mathbf{q}}$ allows to damp the null-space motion. The control law (2) is, therefore, modified as follows:

$$\boldsymbol{\tau} = \mathbf{B}(\mathbf{q})\boldsymbol{\gamma} + \mathbf{C}(\mathbf{q},\dot{\mathbf{q}}) + \mathbf{g}(\mathbf{q}) + \boldsymbol{\tau}_f(\mathbf{q},\dot{\mathbf{q}}) + \boldsymbol{\tau}_R. \tag{12}$$

The control torque $\boldsymbol{\tau}_R$ acts in the null-space of the manipulator, *i.e.*, not affecting the Cartesian motion of the robot. Indeed, the Cartesian controlled robot behavior in (10) is not affected by this term.

IV. Sensorless Extended Kalman Filter

In order to design and implement the sensorless optimal LQR interaction controller, a sensorless model-based methodology (considering the robot-environment interaction dynamics) to estimate the stiffness of the interaction environment is required. In the present paper, an Extended Kalman Filter (EKF) is proposed for this purpose. Since the aim of the paper is to track the translational reference force, only the translational Cartesian DoFs will be considered in the following section for estimation of the environment stiffness.

A. Interaction environment dynamics modeling

In order to design the EKF to be used for the estimation of the interaction environment stiffness, the dynamics of an interaction environment has to be modeled. Based on [34], the simplest way to describe the interaction environment dynamics along translational DoFs is the linear spring-damper

model (with environment stiffness matrix $\mathbf{K}_e$ and environment damping matrix $\mathbf{D}_e$, both diagonal and positive definite). Under the hypothesis of a stable single contact point (*i.e.*, the robot and the environment are always in contact with $\mathbf{x}_e = \mathbf{x}_t$):

$$\mathbf{D}_e\dot{\mathbf{x}}_t + \mathbf{K}_e\Delta\mathbf{x}_t = \mathbf{f}. \tag{13}$$

Since the identification of the environment damping $\mathbf{D}_e$ is not trivial and it does not affect the stiffness estimation at steady-state, the damping is neglected in the environment dynamics (13), considering a pure elastic dynamics:

$$\mathbf{K}_e\left(\mathbf{x}_t - \mathbf{x}^0_{e,t}\right) = \mathbf{f}. \tag{14}$$

where $\mathbf{x}^0_{e,t}$ is the equilibrium position of the environment. $\mathbf{x}^0_{e,t}$ has to be estimated during the target task execution, by defining an appropriate procedure as later described in Section VI. After its estimation, it is possible to translate the task reference frame in the $\mathbf{x}^0_{e,t}$ position to have $\mathbf{x}^0_{e,t} = \mathbf{0}$, simplifying the equations of environment interaction dynamics.

It should be noted that, by neglecting the damping in the proposed environment dynamics (14), a conservative modeling of the robot-environment interaction dynamics is provided in terms of robustness for control purposes. In fact, the real environment damping will increase the stability of the coupled controlled system.

By substituting (14) in (10), the coupled robot-environment interaction dynamics can be defined as:

$$\overline{\mathbf{M}}_t\ddot{\mathbf{x}}_t + \overline{\mathbf{D}}_t\dot{\mathbf{x}}_t + \overline{\mathbf{K}}_t(\mathbf{q})\mathbf{x}_t = \mathbf{K}_t\mathbf{x}^d_t, \tag{15}$$

where $\overline{\mathbf{M}}_t = \mathbf{M}_t$, $\overline{\mathbf{D}}_t = \mathbf{D}_t$, $\overline{\mathbf{K}}_t(\mathbf{q}) = \mathbf{K}_t + \overline{\mathbf{L}}(\mathbf{q})\mathbf{K}_e$. It should be noted that the equivalent stiffness matrix $\overline{\mathbf{K}}_t(\mathbf{q})$ is a function of the joint position $\mathbf{q}$.

B. Extended Kalman Filter design

By exploiting the coupled robot-environment dynamic equation (15), it is possible to design the EKF to be used for the estimation of the interaction environment stiffness $\mathbf{K}_e$.
The robot-environment interaction dynamics can be defined by the following filter state $\mathbf{x}_a$ composed of robot velocity $\dot{\mathbf{x}}_t$ and position $\mathbf{x}_t$ states, and augmented with the environment stiffness properties $\mathbf{K}_e$:

$$\mathbf{x}_a = [\dot{\mathbf{x}}_t, \mathbf{x}_t, \mathbf{K}_e]^T. \tag{16}$$

Substituting the augmented state $\mathbf{x}_a$ (16) in the interaction dynamics model (15), the filter dynamics result in:

$$\mathbf{f}(\mathbf{x_a}, \boldsymbol{\nu_a}) = \begin{bmatrix} \ddot{\mathbf{x}}_t \\ \dot{\mathbf{x}}_t \\ \dot{\mathbf{K}}_e \end{bmatrix} = \begin{bmatrix} \overline{\mathbf{M}}_t^{-1}\left(-\overline{\mathbf{D}}_t\dot{\mathbf{x}}_t - \overline{\mathbf{K}}_t(\mathbf{q})\mathbf{x}_t + \mathbf{K}_t\mathbf{x}^d_t + \boldsymbol{\nu}_{\mathbf{x}_t}\right) \\ \dot{\mathbf{x}}_t + \boldsymbol{\nu}_{\dot{\mathbf{x}}_t} \\ \boldsymbol{\nu}_{\mathbf{K}_e} \end{bmatrix}, \tag{17}$$

where the vector $\boldsymbol{\nu}_a = [\boldsymbol{\nu}_{\mathbf{x}_t}, \boldsymbol{\nu}_{\dot{\mathbf{x}}_t}, \boldsymbol{\nu}_{\mathbf{K}_e}]^T$ accounts for uncertainties in models parameters/estimates.
The observer of the augmented state is therefore defined as:

$$\begin{cases} \dot{\widehat{\mathbf{x}}}_a = \mathbf{f}(\mathbf{x_a}, \boldsymbol{\nu_a}) + \mathbf{K}_{EKF}(\mathbf{y} - \mathbf{C}_a\widehat{\mathbf{x}}_a), \\ \widehat{\mathbf{y}} = \mathbf{h}(\mathbf{x}_a, \mathbf{w}), \end{cases} \tag{18}$$

with $\widehat{\mathbf{x}}_a$ the augmented state estimate. $\mathbf{C}_a$ the observation matrix for the robot velocity $\dot{\mathbf{x}}_t$ and the robot position $\mathbf{x}_t$:

$$\mathbf{C}_a = \begin{bmatrix} \mathbf{I}_{3x3} & \mathbf{0}_{3x3} & \mathbf{0}_{3x3} \\ \mathbf{0}_{3x3} & \mathbf{I}_{3x3} & \mathbf{0}_{3x3} \end{bmatrix}. \tag{19}$$

$\mathbf{h}(\mathbf{x}_a, \mathbf{w})$ defines the relation between measured $\mathbf{y}$ and states $\mathbf{x}_a$ variables. $\mathbf{K}_{EKF}$ the gain matrix:

$$\mathbf{K}_{EKF} = \mathbf{P}\mathbf{C}_a\mathbf{R}^{-1}. \tag{20}$$

$\mathbf{R}$ is the measurement noise matrix defined as:

$$\mathbf{R} = \mathbf{H}E\{\mathbf{w}\mathbf{w}^T\}\mathbf{H}^T = \mathbf{H}\mathbf{W}\mathbf{H}^T, \tag{21}$$

where the observation function $\mathbf{h}$ linearly maps the sample inaccuracies, due to measurement noise $\mathbf{w}$, through the matrix $\mathbf{H}$:

$$\mathbf{H} = \left.\frac{\partial\mathbf{h}}{\partial\mathbf{w}}\right|_{\widehat{\mathbf{x}}_a} = \begin{bmatrix} \mathbf{I}_{3x3} & \mathbf{0}_{3x3} & \mathbf{0}_{3x3} \\ \mathbf{0}_{3x3} & \mathbf{I}_{3x3} & \mathbf{0}_{3x3} \end{bmatrix}. \tag{22}$$

The covariance matrix $\mathbf{P}$ and its rate, as in:

$$\dot{\mathbf{P}} = \mathbf{A}_a\mathbf{P} - \mathbf{P}\mathbf{C}_a^T\mathbf{R}^{-1}\mathbf{C}_a\mathbf{P} + \mathbf{Q} + \mathbf{P}\mathbf{A}_a^T, \tag{23}$$

are based on the dynamics of the state and the model uncertainties, defined with matrix $\mathbf{A}_a$ and matrix $\mathbf{G}_a$ respectively:

$$\mathbf{A}_a = \left.\frac{\partial\mathbf{f}}{\partial\mathbf{x}_a}\right|_{\widehat{\mathbf{x}}_a} \begin{bmatrix} -\overline{\mathbf{M}}_t^{-1}\overline{\mathbf{D}}_t & -\overline{\mathbf{M}}_t^{-1}\overline{\mathbf{K}}_t(\mathbf{q}) & -\overline{\mathbf{M}}_t^{-1}\overline{\mathbf{L}}(\mathbf{q})\mathbf{x}_t \\ \mathbf{I}_{3x3} & \mathbf{0}_{3x3} & \mathbf{0}_{3x3} \\ \mathbf{0}_{3x3} & \mathbf{0}_{3x3} & \mathbf{0}_{3x3} \end{bmatrix}; \tag{24}$$

$$\mathbf{G}_a = \left.\frac{\partial\mathbf{f}}{\partial\boldsymbol{\nu}_a}\right|_{\widehat{\mathbf{x}}_a} = \begin{bmatrix} \mathbf{I}_{3x3} & \mathbf{0}_{3x3} & \mathbf{0}_{3x3} \\ \mathbf{0}_{3x3} & \mathbf{I}_{3x3} & \mathbf{0}_{3x3} \\ \mathbf{0}_{3x3} & \mathbf{0}_{3x3} & \mathbf{I}_{3x3} \end{bmatrix}. \tag{25}$$

In addition, matrix $\mathbf{Q}$ has to be selected to solve (23), which is defined as:

$$\mathbf{Q} = \mathbf{G}_aE\{\boldsymbol{\nu}_a\boldsymbol{\nu}_a^T\}\mathbf{G}_a^T = \mathbf{G}_a\mathbf{V}\mathbf{G}_a^T. \tag{26}$$

It should be noted that in the filter dynamics (17), the equivalent stiffness matrix $\overline{\mathbf{K}}_t(\mathbf{q})$ appears as a function of the joint position $\mathbf{q}$. Analyzing the definition of $\overline{\mathbf{K}}_t(\mathbf{q})$, the joint position dependence is due to the matrices $\mathbf{J}(\mathbf{q})$ and $\mathbf{B}(\mathbf{q})$. When the robot is in interaction with an environment while executing a task (*e.g.*, an assembly task), its joint configuration is not excessively modifying, or at least such modification is happening with a dynamics much slower than the interaction dynamics. It is therefore possible to neglect the time-derivative $\overline{\mathbf{K}}_t(\mathbf{q})$ in (24), considering the constant matrix $\overline{\mathbf{K}}_t(\overline{\mathbf{q}})$, updating $\overline{\mathbf{q}} = \mathbf{q}$ as soon as the robot joint configuration modifications affect the values of $\mathbf{J}(\mathbf{q})$ and $\mathbf{B}(\mathbf{q})$. In this way, (17) can be written as follows:

$$\mathbf{f}(\mathbf{x_a}, \boldsymbol{\nu_a}) = \begin{bmatrix} \ddot{\mathbf{x}}_t \\ \dot{\mathbf{x}}_t \\ \dot{\mathbf{K}}_e \end{bmatrix} = \begin{bmatrix} \overline{\mathbf{M}}_t^{-1}\left(-\overline{\mathbf{D}}_t\dot{\mathbf{x}}_t - \overline{\mathbf{K}}_t(\overline{\mathbf{q}})\mathbf{x}_t + \mathbf{K}_t\mathbf{x}^d_t + \boldsymbol{\nu}_{\mathbf{x}_t}\right) \\ \dot{\mathbf{x}}_t + \boldsymbol{\nu}_{\dot{\mathbf{x}}_t} \\ \boldsymbol{\nu}_{\mathbf{K}_e} \end{bmatrix}. \tag{27}$$

The approximation of $\overline{\mathbf{K}}_t(\mathbf{q})$ in $\overline{\mathbf{K}}_t(\overline{\mathbf{q}})$ introduces negligible modeling errors, that are of orders of magnitude smaller than common modeling errors resulting from the robot dynamics identification procedures.

The estimated environment stiffness $\widehat{\mathbf{K}}_e$ can therefore be computed from (18).

V. Outer sensorless interaction controller

Exploiting the designed inner sensorless Cartesian impedance control (Section III) and the designed EKF (Section IV), the outer interaction controller can be designed. Two main components can be highlighted in the outer controller definition: the coupling compensator $\mathbf{x}_{t,comp}$ and the optimal LQR interaction controller $\mathbf{x}_{t,opt}$. While the coupling compensator allows the controller to deal with the coupled dynamics resulting from the inner sensorless Cartesian impedance controller (10), the optimal LQR interaction control allows the controller to track the reference force by exploiting estimated environment stiffness $\widehat{\mathbf{K}}_e$ (18). These two contributions are used in order to update the inner sensorless Cartesian impedance control setpoint $\mathbf{x}_t^d$ in (10):

$$\mathbf{x}_t^d = \mathbf{x}_t + \mathbf{x}_{t,comp} + \mathbf{x}_{t,opt}. \tag{28}$$

In the following, the two control actions are described. Each Cartesian DoF can be treated independently. Therefore, the following formulation will consider a single-DoF (*i.e.*, scalar quantities).

A. Outer coupling compensator

The coupling compensator $\mathbf{x}_{t,comp}$ allows the controller to deal with the coupled dynamics resulting from the inner sensorless Cartesian impedance controller (10). As resulting from (15), the term $\overline{\mathbf{L}}(\mathbf{q})$ multiplies with an environment stiffness $\mathbf{K}_e$, coupling the dynamic equations. As described in Section IV-B, the update of $\overline{\mathbf{q}} = \mathbf{q}$ can be considered as soon as the modification in robot joint configuration affect the values of $\mathbf{J}(\mathbf{q})$ and $\mathbf{B}(\mathbf{q})$.

The coupling compensator can therefore be defined as:

$$x_{t,comp,i} = \overline{L}_{i,j}\widehat{K}_e^j x_{t,j} + \overline{L}_{i,k}\widehat{K}_e^k x_{t,k}, \tag{29}$$

where i defines the controlled Cartesian DoF, while j and k the coupled Cartesian DoFs.

Substituting (29) in (28), the coupling effect in (15) can be compensated.

B. Outer optimal LQR interaction control

The proposed controller has to perform the force tracking, optimizing the control gains to achieve a fast dynamics for the controlled robot and zero steady-state force error.

Considering the controlled Cartesian DoF i, the following structure has been proposed for the outer interaction controller $x_{t,opt,i}$:

$$x_{t,opt,i} = G_{opt,1,i}\dot{x}_{t,i} + G_{opt,2,i}x_{t,i} - G_{opt,3,i}\int \widehat{e}_{f,i}, \tag{30}$$

where $\widehat{e}_{f,i} = f_i^d - \widehat{f}_i = f_i^d - \widehat{K}_{e,i}x_{t,i}$ is the force error, with f_i^d the reference force and $\widehat{f}_i = \widehat{K}_{e,i}x_{t,i}$ the estimated interaction force based on the estimated environment stiffness $\widehat{K}_{e,i}$. The control loop displays, therefore, three regulators: $G_{opt,1,i}$ is the control gain on the feedback velocity of the robot $\dot{x}_{t,i}$, $G_{opt,2,i}$ is the control gain on the feedback position $x_{t,i}$ of the robot, and $G_{opt,3,i}$ is the control gain of the integral of the force tracking error $e_{f,i}$. These control gains have to be computed by exploiting the optimal LQR control technique [35].

Considering the coupled robot-environment dynamics resulting from (10), (14), (28), and (29), the corresponding state-expression results in:

$$\begin{bmatrix} \dddot{x}_{t,i} \\ \ddot{x}_{t,i} \\ \dot{e}_{f,i} \end{bmatrix} = \begin{bmatrix} -\frac{\widehat{D}_{t,i}}{M_{t,i}} & -\frac{\widehat{K}_{e,i}}{M_{t,i}} & 0 \\ 1 & 0 & 0 \\ 0 & -\widehat{K}_{e,i} & 0 \end{bmatrix} \begin{bmatrix} \ddot{x}_{t,i} \\ \dot{x}_{t,i} \\ e_{f,i} \end{bmatrix} + \begin{bmatrix} \frac{K_{t,i}}{M_{t,i}} \\ 0 \\ 0 \end{bmatrix} \dot{x}_{t,opt,i}, \tag{31}$$

that can be re-written the matricial form:

$$\dot{\boldsymbol{\eta}}_i = \mathbf{A}_i\boldsymbol{\eta}_i + \mathbf{b}_i\dot{x}_{t,opt,i}. \tag{32}$$

From (31) it can be seen that the coupling effect of the $\overline{\mathbf{L}}$ matrix is compensated by the control action (29).

In order to design the optimal LQR interaction controller, J_{cost} is chosen to be the controller performance index:

$$J_{cost,i} := \int_0^\infty \left(\boldsymbol{\eta}_i^T \mathbf{Q}_{opt,i}\boldsymbol{\eta}_i + (\dot{x}_{t,opt,i})^2 \right) dt. \tag{33}$$

$\mathbf{Q}_{opt,i} := diag\,(0, 0, q_i)$ is the LQR gain matrix, where $q_i > 0$ can be tuned in order to modulate the control gains. The state is optimized w.r.t. the force error, *i.e.*, $\boldsymbol{\eta}_i^T \mathbf{Q}_{opt,i}\boldsymbol{\eta}_i = q_i\widehat{e}_{f,i}^2$ for the one DoF problem in (32). The optimal controller with the action $\dot{x}_{t,opt,i}$ is obtained by solving the related minimization problem:

$$J_i^*(\boldsymbol{\eta}_i) := \min_{\dot{x}_{t,opt,i}} \{J_{cost,i}(\boldsymbol{\eta}_i)\}. \tag{34}$$

Under the assumptions of the Linear Quadratic Regulator (LQR) problem [35], resolving (34) corresponds to solve the related Riccati matrix equation:

$$\mathbf{0} = \mathbf{S}_i\mathbf{A}_i + \mathbf{A}_i^T\mathbf{S}_i + \mathbf{Q}_i - \mathbf{S}_i\mathbf{b}_i\mathbf{b}_i^T\mathbf{S}_i, \tag{35}$$

where $\mathbf{S}_i = \mathbf{S}_i^T$ is the solution of (35) (symmetric and positive semi-definite constant 3x3 matrix), so that:

$$\dot{x}_{t,opt,i} = -\mathbf{b}_i^T\mathbf{S}_i\boldsymbol{\eta}_i. \tag{36}$$

The solution $\mathbf{S}_i$ can be analytically computed as a function of the coupled robot-environment system parameters, *i.e.*, as a function of the estimated environment stiffness. In this way, the control gains can be computed and updated at each control step. From (35) and defining $\omega_i = \sqrt{\frac{K_{t,i}}{M_{t,i}}}$, the following six algebraic equations can be derived:

$$\begin{cases} 0 = -S_i(1,1)^2\,\omega_i^4 - 2D_{t,i}S_i(1,1)/M_{t,i} + 2S_i(1,2), \\ 0 = -S_i(1,1)\,S_i(1,2)\,\omega_i^4 + S_i(2,2) - \overline{K}_{e,i}S_i(1,3) \\ \quad\; - DS_i(1,2)/M_{t,i} - \overline{K}_{e,i}S_i(1,1)/M_{t,i}, \\ 0 = -S_i(1,1)\,S_i(1,3)\omega_i^4 + S_i(2,3) - DS_i(1,3)/M_{t,i}, \\ 0 = -S_i(1,2)^2\,\omega_i^4 - 2\overline{K}_{e,i}S_i(1,2)/M_{t,i} - 2\overline{K}_{e,i}S_i(2,3), \\ 0 = -S_i(1,2)\,S_i(1,3)\,\omega_i^4 - \overline{K}_{e,i}S_i(3,3) - \overline{K}_{e,i}S_i(1,3)/M_{t,i}, \\ 0 = -S_i(1,3)^2\,\omega_i^4 + q_i. \end{cases} \tag{37}$$

From the sixth equation of (37), $S_i(1,3)$ can be computed as:

$$S_i(1,3) = -\sqrt{q_i}/\omega_i^2. \tag{38}$$

Substituting (38) in (37) gives:

$$\begin{cases} 0 = -S_i(1,1)^2\,\omega_i^4 - 2D_{t,i}\,S_i(1,1)/M_{t,i} + 2S_i(1,2), \\ 0 = -S_i(1,1)\,S_i(1,2)\,\omega_i^4 + S_i(2,2) + \overline{K}_{e,i}\sqrt{q_i}/\omega_i^2 \\ \quad - DS_i(1,2)/M_{t,i} - \overline{K}_{e,i}S_i(1,1)/M_{t,i}, \\ 0 = S_i(1,1)\sqrt{q_i}\omega_i^2 + S_i(2,3) + D\sqrt{q_i}/\left(M_{t,i}\,\omega_i^2\right), \\ 0 = -S_i(1,2)^2\,\omega_i^4 - 2\overline{K}_{e,i}S_i(1,2)/M_{t,i} - 2\overline{K}_{e,i}S_i(2,3), \\ 0 = S_i(1,2)\sqrt{q_i}\,\omega_i^2 - \overline{K}_{e,i}S_i(3,3) - \overline{K}_{e,i} - \sqrt{q_i}/\left(\omega_i^2\,M_{t,i}\right). \end{cases} \tag{39}$$

From the second equation of (39), it is possible to derive $S_i(2,2)$ as:

$$\begin{aligned} S_i(2,2) = {} & \overline{K}_{e,i}S_i(1,1)/M_{t,i} + D_{t,i}\,S_i(1,2)/M_{t,i} \\ & + S_i(1,1)\,S_i(1,2)\,\omega^4 - \overline{K}_{e,i}\sqrt{(q_i)}/\omega_i^2. \end{aligned} \tag{40}$$

With $S_i(2,2)$ given in (40), (39) becomes:

$$\begin{cases} 0 = -S_i(1,1)^2\,\omega_i^4 - 2D_{t,i}\,S_i(1,1)/M_{t,i} + 2S_i(1,2), \\ 0 = S_i(2,3) + S_i(1,1)\,\omega_i^2\sqrt{q_i} + D_{t,i}\sqrt{q}/\left(M_{t,i}\,\omega_i^2\right), \\ 0 = -S_i(1,2)^2\,\omega_i^4 - 2\overline{K}_{e,i}S_i(1,2)/M_{t,i} - 2\overline{K}_{e,i}S_i(2,3), \\ 0 = S_i(1,2)\,\omega_i^2\sqrt{q_i} - \overline{K}_{e,i}S_i(3,3) + \overline{K}_{e,i}\sqrt{q_i}/\left(M_{t,i}\,\omega_i^2\right). \end{cases} \tag{41}$$

Considering the fourth equation of (41), $S_i(3,3)$ can then be calculated as:

$$S_i(3,3) = S_i(1,2)\,\omega_i^2\sqrt{q_i}/\overline{K}_{e,i} + \sqrt{q_i}/\left(M_{t,i}\,\omega_i^2\right). \tag{42}$$

Replacing $S_i(3,3)$ in (41) then gives:

$$\begin{cases} 0 = -S_i(1,1)^2\,\omega_i^4 - 2D_{t,i}\,S_i(1,1)/M_{t,i} + 2S_i(1,2), \\ 0 = S_i(2,3) + S_i(1,1)\,\omega_i^2\sqrt{q_i} + D_{t.i}\sqrt{q_i}/\left(M_{t,i}\,\omega_i^2\right), \\ 0 = -S_i(1,2)^2\,\omega_i^4 - 2\overline{K}_{e,i}S_i(1,2)/M_{t,i} - 2\overline{K}_{e,i}S_i(2,3). \end{cases} \tag{43}$$

$S_i(2,3)$ can be obtained from the second equation of (43) as follows:

$$S_i(2,3) = -D_{t,i}\sqrt{q_i}/\left(M_{t,i}\,\omega_i^2\right) - S_i(1,1)\,\omega_i^2\sqrt{q_i}. \tag{44}$$

Using now $S_i(2,3)$ in (43), the following equations are computed:

$$\begin{cases} 0 = -S_i(1,1)^2\,\omega_i^4 - 2D_{t,i}\,S_i(1,1)/M_{t,i} + 2S_i(1,2), \\ 0 = 2\overline{K}_{e,i}\left(S_i(1,1)\,\omega_i^2\sqrt{q_i} + D_{t,i}\sqrt{q_i}/(M_{t,i}\,\omega_i^2)\right) \\ \quad - S_i(1,2)^2\,\omega_i^4 - 2\overline{K}_{e,i}S_i(1,2)/M_{t,i}. \end{cases} \tag{45}$$

Using the first equation of (45), $S_i(1,2)$ is computed as:

$$S_i(1,2) = S_i(1,1)^2\,\omega_i^4/2 + D_{t,i}\,S_i(1,1)/M_{t,i}. \tag{46}$$

Substituting $S_i(1,2)$ from (46) into (45), the following equation is then obtained:

$$\begin{aligned} 0 = {} & 2\overline{K}_{e,i}\sqrt{q_i}\left(S_i(1,1)\,M_{t,i}\,\omega_i^4 + D_{t,i}\right)/\left(M_{t,i}\,\omega_i^2\right) \\ & - \overline{K}_{e,i}\,S_i(1,1)\left(S_i(1,1)\,M_{t,i}\,\omega_i^4 + 2D_{t,i}\right)/M_{t,i} \\ & - S_i(1,1)^2\,\omega_i^4\left(S_i(1,1)\,M_{t,i}\,\omega_i^4 + 2D_{t,i}\right)^2/\left(4M_{t,i}^2\right). \end{aligned} \tag{47}$$

Finally, (47) can be written in the following form:

$$\begin{aligned} 0 = {} & F_{1,i}\,S_i(1,1)^4 + F_{2,i}\,S_i(1,1)^3 + F_{3,i}\,S_i(1,1)^2 \\ & + F_{4,i}\,S_i(1,1) + F_{5,i}, \end{aligned} \tag{48}$$

where:

$$\begin{cases} F_{1,i} = -\omega_i^{12}/4, \\ F_{2,i} = -\omega_i^8\,D_{t,i}/M_{t,i}, \\ F_{3,i} = -\overline{K}_{e,i}\,\omega_i^4/M_{t,i} - \omega_i^4\,D_{t,i}^2/M_{t,i}^2, \\ F_{4,i} = -2\overline{K}_{e,i}\,D_{t,i}/M_{t,i}^2 + 2\overline{K}_{e,i}\,\omega_i^4\sqrt{q_i}/\omega_i^2, \\ F_{5,i} = 2\overline{K}_{e,i}\,D_{t,i}\sqrt{q_i}/\left(M_{t,i}\,\omega_i^2\right). \end{cases} \tag{49}$$

To solve the fourth order equation, let's define:

$$\begin{cases} p_{1,i} = \left(8F_{1,i}F_{3,i} - 3F_{2,i}^2\right)/\left(8F_{1,i}^2\right), \\ q_{1,i} = \left(F_{2,i}^3 - 4F_{1,i}F_{2,i}F_{3,i} + 8F_{1,i}^2F_{4,i}\right)/\left(8F_{1,i}^3\right), \\ \Delta_{0,i} = F_{3,i}^2 - 3F_{2,i}F_{4,i} + 12F_{1,i}F_{5,i}, \\ \Delta_{1,i} = 2F_{3,i}^3 - 9F_{2,i}F_{3,i}F_{4,i} + 27F_{2,i}^2F_{5,i} + 27F_{1,i}F_{4,i}^2 \\ \qquad - 72F_{1,i}F_{3,i}F_{5,i}, \\ V_i = \sqrt[\frac{1}{3}]{\Delta_{1,i} + \sqrt{\Delta_{1,i}^2 - 4\Delta_{0,i}^3}}/2, \\ N_i = \sqrt{-2/3\,p_{1,i} + (V_i + \Delta_{0,i}/V_i)/(3F_{1,i})}/2. \end{cases} \tag{50}$$

Then, the four solutions of (48) are:

$$\begin{cases} S_i(1,1)^{\#1} = -F_{2,i}/(4F_{1,i}) - N_i \\ \qquad + \sqrt{-4N_i^2 - 2p_{1,i} + q_{1,i}/N_i}/2, \\ S_i(1,1)^{\#2} = -F_{2,i}/(4F_{1,i}) - N_i \\ \qquad - \sqrt{-4N_i^2 - 2p_{1,i} + q_{1,i}/N_i}/2, \\ S_i(1,1)^{\#3} = -F_{2,i}/(4F_{1,i}) + N_i \\ \qquad + \sqrt{-4N_i^2 - 2p_{1,i} - q_{1,i}/N_i}/2, \\ S_i(1,1)^{\#4} = -F_{2,i}/(4F_{1,i}) + N_i \\ \qquad - \sqrt{-4N_i^2 - 2p_{1,i} - q_{1,i}/N_i}/2. \end{cases} \tag{51}$$

The solution resulting real and positive will be selected as $S_i(1,1)$, to allow for the computation of (40), (42), (44), and (46), and to compute (36). The optimal control action $x_{t,i,opt}$ in (30) can finally be computed imposing:

$$\begin{cases} G_{opt,1,i} = -\omega_i^2\,S_i(1,1), \\ G_{opt,2,i} = -\omega_i^2\,S_i(2,1), \\ G_{opt,3,i} = -\omega_i^2\,S_i(3,1). \end{cases} \tag{52}$$

Remark 4. It should be noted that the resulting gains computation can be easily implemented for on-line tuning.

On the basis of the estimated environment stiffness and sensorless Cartesian impedance control parameters, the proposed formulas allow to update the control gains in (52) at each control step.

Remark 5. It is important to note that the outer control loop is interconnected with the EKF (exploiting the provided environment stiffness estimation). Therefore, even though the EKF and the outer control loop are individually stable, the dynamics of the estimation given by the EKF affects the stability of the controller. Thus, it is important that the dynamics of the EKF is faster than the controller dynamics (at least one decade) to avoid any instability resulting from the transient dynamics of the EKF.

VI. Results

In order to show the effectiveness of the proposed control schema, experimental validation is proposed in this Section. A Franka EMIKA panda manipulator has been employed in the proposed experiments. The adopted robot is equipped with torque sensors at joint-level, making it possible to estimate the interaction forces at the robot's end-effector. These measurements are used as ground-truth to validate the interaction force estimation derived from the proposed EKF (Section IV). The Franka EMIKA panda robot torque control (control frequency: 1000 Hz) has been exploited for the implementation of the proposed sensorless Cartesian impedance controller (Section III) with force tracking capabilities (Section V). The robot dynamics compensation is performed on the basis of the inertia matrix $\mathbf{B}(\mathbf{q})$, Coriolis vector $\mathbf{C}(\mathbf{q},\dot{\mathbf{q}})$, and gravity vector $\mathbf{g}(\mathbf{q})$ in the controller (2). These quantities are provided by the model-based controller of the robot at each control step. W.r.t. the compensation of the friction at joint-level $\boldsymbol{\tau}_f(\mathbf{q},\dot{\mathbf{q}})$, the friction modeling in [36] has been exploited, taking into account viscous and Coulomb effects. The LQR interaction control gains are updated every 10 Hz, in order to avoid transition in the estimation provided by the EKF that might cause instabilities in the interaction controller.

The proposed control framework does not include a force/torque sensor, and the estimation of the interaction force relies on the estimation of the environment stiffness (that can be performed only if the robot is in interaction with the environment, see Section IV). Therefore, it is necessary to define a procedure to estimate the environment equilibrium position $\mathbf{x}_{e,t}^0$ to initialize the proposed EKF and force tracking task. To this purpose, the following procedure has been implemented:

- the robot is positioned in proximity of the target environment, some millimeters away from the expected contact point (a distance in a range of $5-10$ mm). In fact, due to uncertainties related to the positioning of the target environment (uncertainties present even in a structured environment, such as industrial plants), the real environment equilibrium position has to be estimated during the task execution;
- a soft, damped, and slow (*i.e.*, with a limited bandwidth) behavior is imposed to the robot's Cartesian impedance controller (with translational stiffness terms lower than 1000 N/m, translational damping ratio terms $\mathbf{h}$ equal to 1, where $\mathbf{D} = 2\mathbf{h}\sqrt{\mathbf{MK}}$, and translational mass terms higher than 20 kg). A constant small setpoint deformation $\Delta\mathbf{x}_t$ is imposed to the cartesian impedance setpoint in the approach direction to the target environment (*i.e.*, imposing $\mathbf{x}_t^d = \mathbf{x}_t + \Delta\mathbf{x}_t$, with $\Delta\mathbf{x}_t \leq 0.5$ mm). The robot, therefore, gently and smoothly moves towards the target environment;
- once the robot and the environment are in contact, with imposed constant small setpoint deformation $\Delta\mathbf{x}_t$, an equilibrium between the robot and the target environment is found, in which limited interaction forces are established. Monitoring the robot's Cartesian position and velocity, it is possible to identify the dynamic-equilibrium establishment. As soon as the equilibrium condition is detected, $\Delta\mathbf{x}_t = 0$ mm is imposed in order to reduce again the interaction force. Then, the estimation of the equilibrium position of the interaction environment $\mathbf{x}_{e,t}^0$ is performed with limited uncertainties.

Exploiting the proposed procedure, it is therefore possible to estimate the equilibrium position of the target environment. After the estimation is performed, the proposed EKF (Section IV) can be initialized, performing the estimation of the environment stiffness property. The provided environment stiffness estimation is used in order to compute the interaction force in (14) to close the force loop (Section V).

Two main tasks have been considered in order to validate the developed control approach: a probing task, and the closing of a plastic (*i.e.*, compliant) box with a snap-fit closure mechanism. The second task is particularly interesting since these assembly features are common in many applications [37], [38]. The snap-fit closure mechanism requires the robot to overcome the closing force to perform the task, while avoiding too high force that could result in breaking the part. Therefore, an accurate force controller is needed. The different environments stiffness values have been calibrated making use of a dynamometer. The proposed tasks are divided into three main phases:

- approaching phase: the robot starts its motion to approach the target environment, establishing the contact, and estimating the environment equilibrium position;
- estimation phase: the EKF is enabled and the environment stiffness and, therefore, the interaction force are estimated. The estimated environment stiffness $\widehat{K}_{e,z}$ is initialized in order to compute the LQR optimal control gains for force tracking purposes;
- force tracking phase: the proposed controller is enabled and the reference force is tracked.

For both tasks, the following Cartesian impedance control parameters have been imposed during the force tracking application: mass parameters of $\mathbf{M}$ have been imposed to 10 kg, the inertia parameters to 10 kg m^2; the translational and the rotational parameters of $\mathbf{K}$ have been imposed to 1000 N/m and 5000 Nm/rad, respectively; the translational and rotational parameters of the damping ratio diagonal matrix $\mathbf{h}$ have been imposed to 1. In the following, the results related to the two tasks are analyzed.

Remark 6. The EKF dynamics have been tuned experimentally in order to achieve the fastest estimation performance.

A. Probing task

As a first experiment, a probing task has been performed. The robot has to establish a controlled interaction with the target environment, guaranteeing the tracking of a reference force. The main direction of the task is the vertical z direction, *i.e.*, the robot establishing the interaction along this Cartesian DoF.

Two different environments have been tested: a soft environment $K_{e,z}^{soft}$, and a stiff environment $K_{e,z}^{stiff}$.

Two different values of the LQR control gains q have been tested: $q = q^{\#1} = 0.00001$ and $q = q^{\#2} = 0.0001$. The q gain, in fact, allows to modify the force tracking performance (*i.e.*, the controller bandwidth) for the controlled robot.

Stiffness estimation results for both the target environments and for both the applied LQR gains $q^{\#1}$ and $q^{\#2}$ are shown respectively in Figure **??** for the soft environment $K_{e,z}^{soft}$, and in Figure **??** for the stiff environment $K_{e,z}^{stiff}$. Estimation performance is highlighted, indicating the method is able to provide an estimation with limited error w.r.t. the calibrated environment stiffness $K_{e,z}$. $\widehat{\overline{K}}_{e,z}$ is highlighted in order to show the initialized condition for the computation of the LQR optimal control gains. Figure **??** and Figure **??** show the force tracking results w.r.t. the soft environment $K_{e,z}^{soft}$, considering the LQR gain $q^{\#1}$ and $q^{\#2}$, respectively. Left side of the figure **??** and Figure **??** show the estimated interaction force $\widehat{f}_z$ vs. the measured interaction force f_z, together with the reference force f_z^d. As it can be seen, the defined three task phases can be clearly identified. It can be highlighted that the initial established measured force f_z is relatively small (less than 5 N), providing the proof that the proposed approach for the environment equilibrium position estimation is effective. In addition, the faster force control bandwidth achieved by applying the higher LQR gain $q^{\#2}$ w.r.t. $q^{\#1}$ is shown, highlighting the effect of the parameter q on the control performance. Right side of the figure **??** and Figure **??** show the interaction force estimation error $\widehat{e}_{f,z} = f_z - \widehat{f}_z$. As it can be seen, the achieved estimation dynamics is fast, and small estimation errors are achieved. Figure **??** and Figure **??** show the force tracking results w.r.t. the stiff environment $K_{e,z}^{stiff}$, considering the LQR gain $q^{\#1}$ and $q^{\#2}$, respectively. As for the soft environment, left side of the figure **??** and Figure **??** show the estimated interaction force $\widehat{f}_z$ vs. the measured interaction force f_z, together with the reference force f_z^d. As previously highlighted, the initial established measured force f_z is relatively small in the approaching phase (less than 5 N). Also in this case, a faster force control bandwidth is achieved by applying the higher LQR gain $q^{\#2}$ w.r.t. $q^{\#1}$. Right side of the figure **??** and Figure **??** show the interaction force's estimation error $\widehat{e}_{f,z} = f_z - \widehat{f}_z$, highlighting the small estimation error in the task execution.

B. Closing of a plastic box

As a second experiment, the closing of a plastic (*i.e.*, compliant) box is performed by the robot. Similarly to the probing task, the robot has to establish the interaction with the target part along the z vertical direction. The closing of the plastic box is based on a snap-fit mechanism, *i.e.*, requiring a target force to perform the task. Therefore, the robot has to apply a reference controlled force in order to achieve the closure of the box without breaking it. A video of the proposed application is available at https://youtu.be/YVHeEzqbfbU.

The LQR control gain $q = 0.00001$ has been tested within the target task.

Stiffness estimation results for the target application are shown in Figure **??** for the plastic box $K_{e,z}^{box}$. As it can be seen, the EKF is capable of estimating the box stiffness with a fast dynamics and limited errors. $\widehat{\overline{K}}_{e,z}$ is highlighted in order to show the initialized condition for the computation of the LQR optimal control gains. Figure **??** shows the force tracking results. Left side shows the estimated interaction force $\widehat{f}_z$ vs. the measured interaction force f_z, together with the reference force f_z^d. The defined three task phases can be clearly identified from the force data. The initial established measured force f_z is relatively small (less than 5 N), *i.e.*, the proposed approach allows to estimate the equilibrium position of the environment with limited uncertainties. Right side of the figure shows the interaction force estimation error $\widehat{e}_{f,z} = f_z - \widehat{f}_z$. The achieved estimation dynamics is fast, and small estimation errors are achieved.

VII. Enhancing the controller by the design of an external wrench observer

An external wrench observer can be designed to enhance the performance of the proposed controller. In particular, such an observer can be exploited to eliminate the hypothesis of a stable single contact point of interaction between the robot and the environment, making it possible to execute contact-motion tasks (*e.g.*, polishing tasks), *i.e.*, controlling the normal force while moving on a target surface. In such a way, the detection of no contact/contact (and vice versa) transitions is possible, thus, enabling the environment stiffness EKF in Section IV-B as soon as a steady interaction is achieved. The steady interaction is considered to be achieved as soon as the variation of the estimated force is less than 1 N for 3 consecutive seconds. Therefore, the procedure for the estimation of the environment equilibrium position $\mathbf{x}_{e,t}^0$ described in Section VI is no longer required.

The proposed EKF in Section IV-B is adapted in order to perform the estimation of the external wrench (*i.e.*, both external forces and torques) applied on the robot. To this end, the augmented state $\mathbf{x}_a$ in (16) is modified to:

$$\mathbf{x}_a = [\dot{\mathbf{x}}, \Delta\mathbf{x}, \mathbf{h}_{ext}]^T. \tag{53}$$

The filter dynamics in (27) is, therefore, modified as follows:

$$\mathbf{f}(\mathbf{x_a}, \boldsymbol{\nu}) = \begin{bmatrix} \ddot{\mathbf{x}} \\ \dot{\mathbf{x}} \\ \dot{\mathbf{h}}_{ext} \end{bmatrix} = \begin{bmatrix} \mathbf{M}^{-1}\left(-\mathbf{D}\dot{\mathbf{x}} - \mathbf{K}\mathbf{x} + \overline{\mathbf{L}}(\mathbf{q})\mathbf{h}_{ext} + \mathbf{K}\mathbf{x}^d + \boldsymbol{\nu}_{\mathbf{x}}\right) \\ \dot{\mathbf{x}} + \boldsymbol{\nu}_{\dot{\mathbf{x}}} \\ \boldsymbol{\nu}_{\mathbf{h}_{ext}} \end{bmatrix}, \tag{54}$$

Following the same procedure described in Section IV-B for the derivation of the EKF, (54) can be employed to estimate

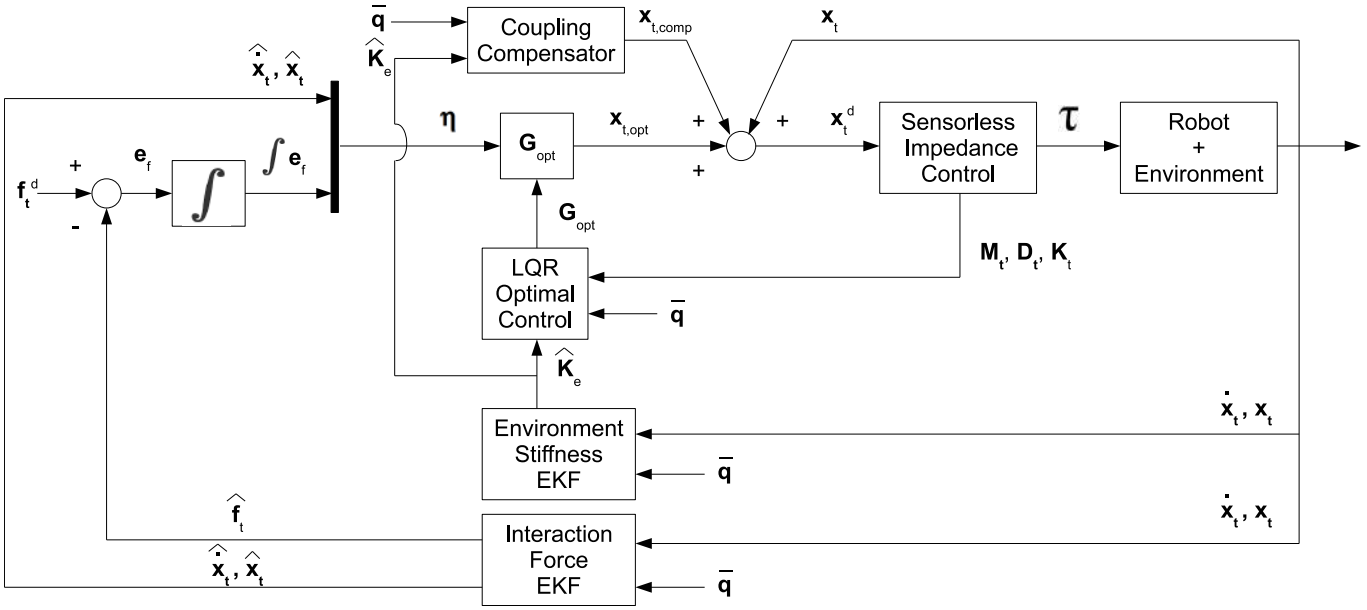

Fig. 1: Proposed modified control schema highlighting the main components: (i) sensorless Cartesian impedance control, (ii) inner Extended Kalman Filter for the environment stiffness estimation, (iii) inner Extended Kalman Filter for the interaction force estimation, (iv) outer coupling compensator, and (v) outer LQR optimal interaction controller.

the external wrench on the robot for the execution of the target interaction task. It has to be noted that (54) considers both the translational and the rotational DoFs, *i.e.*, making it possible to estimate the external wrench (both forces and torques).

The modified control schema is shown in Figure 1.

In the following, two tasks are proposed for the validation of the proposed approach enhanced by the external wrench observer: a polishing-like task and an assembly task of a gear into its shaft.

Remark 7. It is important to note that the outer control loop is now interconnected with both the EKF for the environment stiffness estimation, and the EKF for the interaction force estimation (Figure 1). Therefore, even though the EKFs and the outer control loop are individually stable, the dynamics of the estimations affect the stability of the controller. Thus, it is important that the dynamics of the EKFs are faster than the controller dynamics (at least one decade) to avoid any instability resulting from the transient dynamics of the EKFs.

Remark 8. The proposed modified control schema allows to implement two independent observers, one for the estimation of the environment stiffness, and the other for the interaction force (Figure 1). This means that the two EKFs are not interconnected, *i.e.*, the output of each EKF is used only for control purposes (not for estimation purposes). An EKF for the environment stiffness estimation might be designed exploiting the estimated interaction force provided by the other EKF (similarly to [39]). However, such an interconnection might affect the performance and the stability of the cascade observers schema. While some works deal with the cascade observers design [40]–[42], the implementation of these methodologies introduces additional complexity for real applications.

A. Polishing-like task

The proposed task is to approach the target environment along the robot's z direction. Then, the robot has to maintain a constant contact with the environment by applying a reference force f_z^d, while sliding along directions x and y. The reference force has been imposed as $f_z^d = 30$ N. The controller in (28) has been exploited to track the reference force f_z^d. A sinusoidal motion has been imposed along directions x and y. The impedance control matrices have been initialized as in Section VI, with the LQR control gain imposed to $q = 0.00001$.

Figure 2 shows in the first column the estimated interaction force $\widehat{f}_z$ vs. the measured interaction force f_z, also highlighting the reference force f_z^d. The second column shows the interaction force estimation error $\widehat{e}_{f,z} = f_z - \widehat{f}_z$. Limited errors are shown, comparable to state-of-the-art techniques for sensorless external force estimation. A fast estimation is achieved, making it possible to estimate the interaction force while performing the task. Spikes in the estimated interaction force (due to the transition phases) are filtered by the slower dynamics of the outer controller (w.r.t. the one implemented for the EKF), thus, achieving a stable interaction between the robot and the environment. Figure 3 shows the performed estimation of the interaction environment stiffness, enabled as soon as the steady interaction is achieved.

B. Assembly task

The proposed task is to assemble a gear onto its shaft. The target task is shown in Figure 4. The Siemens assembly task has been considered, producing the required 3D printed components. The CAD files of the parts can be found at the link https://new.siemens.com/us/en/company/fairs-events/robot-learning.html. The direction of the main task is z and,

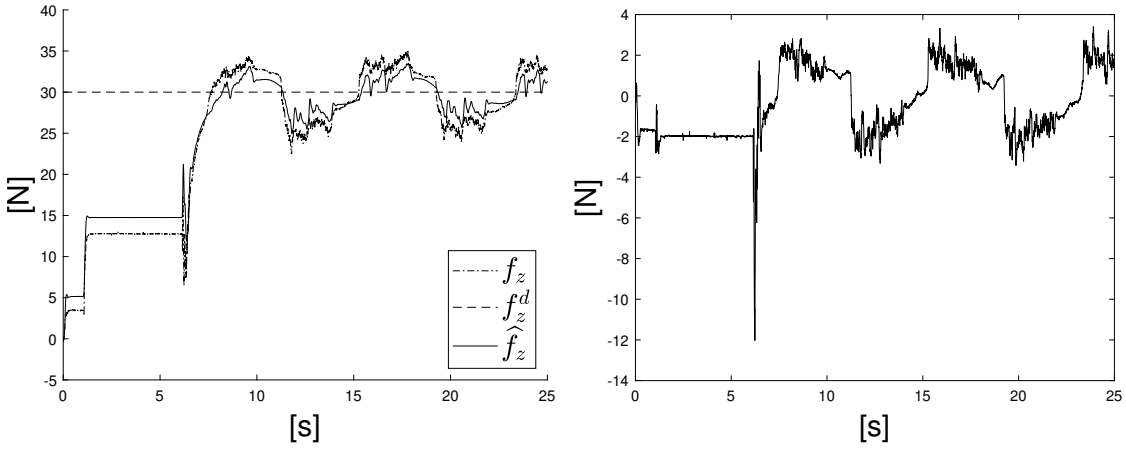

(a) $\widehat{f}_z$ vs. f_z (b) $\widehat{e}_{f,z}$

Fig. 2: Results related to the LQR force tracking controller for the polishing-like task. (a) estimated interaction force $\widehat{f}_z$ (continuous line) vs. measured interaction force f_z (dot-dashed line). Reference force f_z^d (dashed line) is highlighted. (b) estimated interaction force error $\widehat{e}_{f,z}$. The contact is achieved after ≈ 1.5 s, and the steady contact is achieved after ≈ 5.5 s.

therefore, a reference force $f_z^d = 30$ N has been defined to perform the insertion task. The controller in (28) has again been exploited to track the reference force f_z^d. The sensorless Cartesian impedance control is exploited in order to have the robot compliant along the other Cartesian DoFs. The impedance control matrices have been initialized as in Section VI. The LQR control gain $q = 0.00001$ has been imposed.

Figure 5 shows in the first column the estimated interaction force $\widehat{f}_z$ vs. the measured interaction force f_z, also highlighting the reference force f_z^d. The second column shows the interaction force estimation error $\widehat{e}_{f,z} = f_z - \widehat{f}_z$. Limited steady state errors (around 2 N) are shown, comparable to state-of-the-art techniques for sensorless external force estimation. A fast estimation is achieved, showing the convergence of the estimation in approximately 0.1 s, as it can be seen from the interaction force estimation error plots. The estimated environment stiffness is shown in Figure 6. The estimation is performed as soon as a steady interaction is achieved in the proposed experiment.

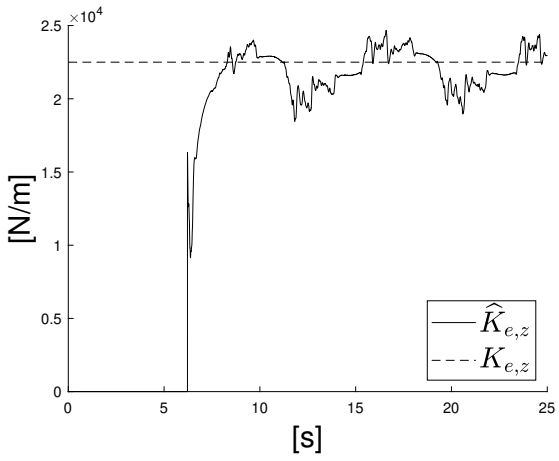

Fig. 3: Environment stiffness $K_{e,z}$ estimation results for the polishing-like task. The estimated environment stiffness $\widehat{K}_{e,z}$ (continuous line) vs. the calibrated environment stiffness $K_{e,z}$ (dashed line) is shown.

VIII. Conclusions and Future Work

The present paper proposed a methodology for the design of an interaction control applied to the sensorless industrial robots. The framework involves an inner sensorless Cartesian impedance controller to achieve a compliant controlled robot behavior without the use of wrench signals. An EKF is then derived in order to estimate the environment stiffness, to be exploited by the outer control schema for force tracking capabilities. Two main control actions are defined: a coupling compensator and an optimal LQR interaction controller. The

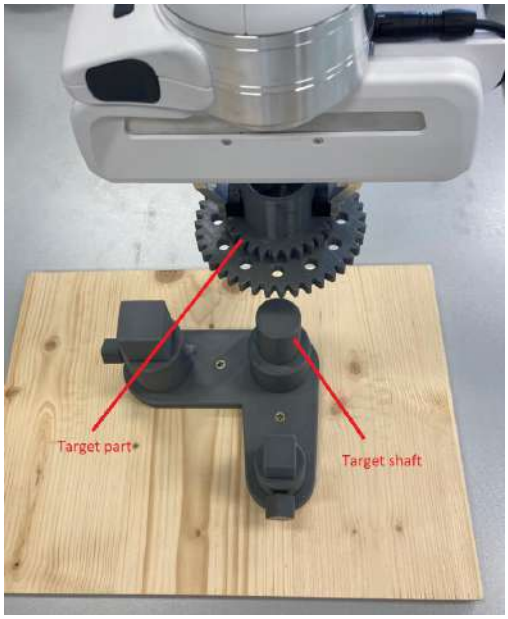

Fig. 4: Experimental set-up including the Franka EMIKA panda manipulator for the target assembly task. The manipulated gear and its shaft are highlighted. The shaft structure has been fixed to the same table on which the robot is mounted.

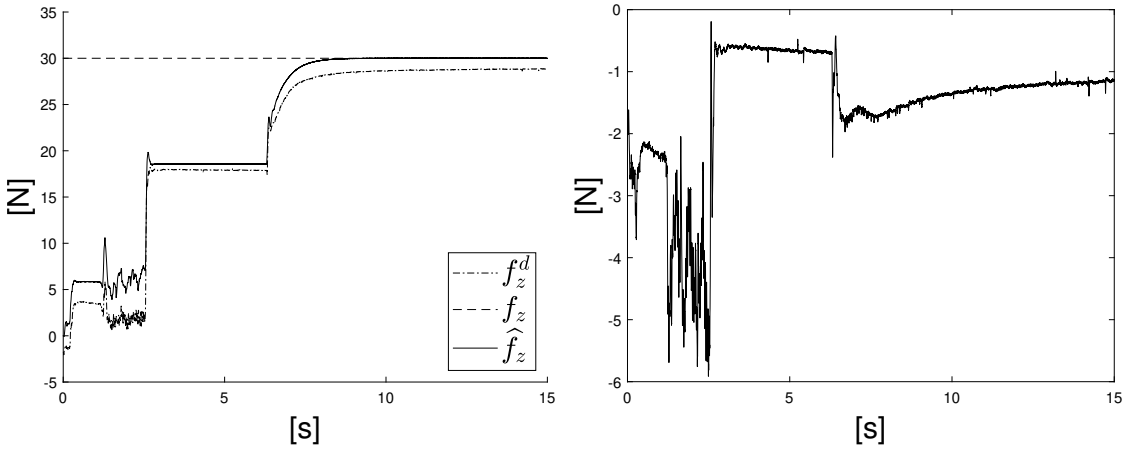

(a) $\widehat{f}_z$ vs. f_z (b) $\widehat{e}_{f,z}$

Fig. 5: Results related to the LQR force tracking controller for the assembly task. (a) estimated interaction force $\widehat{f}_z$ (continuous line) vs. measured interaction force f_z (dot-dashed line). Reference force f_z^d (dashed line) is highlighted. (b) estimated interaction force error $\widehat{e}_{f,z}$. The contact is achieved after ≈ 3.5 s, and the steady contact is achieved after ≈ 6.5 s.

former control action compensates for the coupled dynamics resulting from the sensorless Cartesian impedance controller. The latter control action exploits the environment stiffness estimation to compute (on the basis of analytical derivation as a function of the environment stiffness estimation) the interaction control gains online, ensuring stability and optimality of the interaction. The interaction force is estimated by exploiting the environment stiffness estimation to close the force loop. The proposed approach has been validated with experiments, using a Franka EMIKA panda manipulator as a test platform. Two tasks have been considered: a probing task, and the closing of a plastic box with snap-fit closure mechanism. The proposed sensorless EKF is capable of estimating the environment stiffness with limited uncertainties. The proposed interaction controller is able to track the reference force by exploiting the provided environment stiffness estimation, thus, achieving a fast closed-loop bandwidth. To enhance the performance of the proposed controller, an external wrench observer is derived, adapting the developed EKF for the environment stiffness estimation. The developed wrench observer allows one to eliminate the hypothesis of a stable single contact point of interaction between the robot and the environment. Such an observer, therefore, gives a signal which can be used to detect no-contact/contact transitions, enabling the EKF for the environment stiffness estimation as needed. Two tasks have been considered to validate the improved control framework: a polishing-like task and an assembly task. The developed observer is capable of estimating the external interaction force, thereby making it possible to initialize the estimation of the environment stiffness as soon as the steady interaction is achieved.

Future work is devoted to investigate machine learning techniques for local friction models identification to improve the adopted modeling, by verifying the influence of interaction force and joint temperature. The optimal redundancy management of the manipulator is also under consideration. Finally, optimizing the tuning of the impedance control gains, optimal LQR interaction control gains, and EKF gains is under investigation, making use of machine learning techniques.

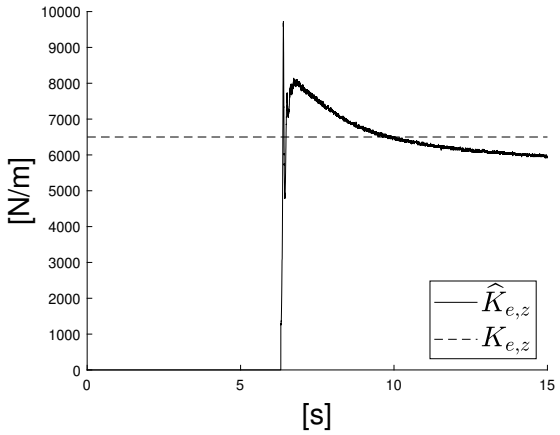

Fig. 6: Environment stiffness $K_{e,z}$ estimation results for the assembly task. The estimated environment stiffness $\widehat{K}_z$ (continuous line) vs. the calibrated environment stiffness K_z (dashed line) is shown.

REFERENCES

[1] M. Ben-Ari and F. Mondada, "Robots and their applications," in *Elements of Robotics*. Springer, 2018, pp. 1–20.

[2] S. Dattaprasad and Y. V. Rao, "A survey of various robot learning techniques," *International Journal of Pure and Applied Mathematics*, vol. 118, no. 20, 2018.

[3] Z. M. Mohamed, *Flexible Manufacturing Systems: Planning Issues and Solutions*. Routledge, 2018.

[4] N. Hogan, "Impedance control: An approach to manipulation," in *1984 American control conference*. IEEE, 1984, pp. 304–313.

[5] M. Vukobratovic, "Robot-environment dynamic interaction survey and future trends," *Journal of Computer and Systems Sciences International*, vol. 49, no. 2, pp. 329–342, 2010.

[6] L. Roveda, N. Pedrocchi, M. Beschi, and L. M. Tosatti, "High-accuracy robotized industrial assembly task control schema with force overshoots avoidance," *Control Engineering Practice*, vol. 71, pp. 142–153, 2018.

[7] A. Janot, P.-O. Vandanjon, and M. Gautier, "A generic instrumental variable approach for industrial robot identification," *IEEE Transactions on Control Systems Technology*, vol. 22, no. 1, pp. 132–145, 2013.

[8] W.-H. Chen, D. J. Ballance, P. J. Gawthrop, and J. O'Reilly, "A nonlinear disturbance observer for robotic manipulators," *IEEE Transactions on industrial Electronics*, vol. 47, no. 4, pp. 932–938, 2000.

[9] M. Van Damme, P. Beyl, B. Vanderborght, V. Grosu, R. Van Ham, I. Vanderniepen, A. Matthys, and D. Lefeber, "Estimating robot end-effector force from noisy actuator torque measurements," in *2011 IEEE International Conference on Robotics and Automation*. IEEE, 2011, pp. 1108–1113.

[10] A. Colomé, D. Pardo, G. Alenya, and C. Torras, "External force estimation during compliant robot manipulation," in *2013 IEEE International Conference on Robotics and Automation*. IEEE, 2013, pp. 3535–3540.

[11] M. Linderoth, A. Stolt, A. Robertsson, and R. Johansson, "Robotic force estimation using motor torques and modeling of low velocity friction disturbances," in *2013 IEEE/RSJ International Conference on Intelligent Robots and Systems*. IEEE, 2013, pp. 3550–3556.

[12] J. Hu and R. Xiong, "Contact force estimation for robot manipulator using semiparametric model and disturbance kalman filter," *IEEE Transactions on Industrial Electronics*, vol. 65, no. 4, pp. 3365–3375, 2017.

[13] E. Villagrossi, L. Simoni, M. Beschi, N. Pedrocchi, A. Marini, L. M. Tosatti, and A. Visioli, "A virtual force sensor for interaction tasks with conventional industrial robots," *Mechatronics*, vol. 50, pp. 78–86, 2018.

[14] E. Magrini, F. Flacco, and A. De Luca, "Estimation of contact forces using a virtual force sensor," in *2014 IEEE/RSJ International Conference on Intelligent Robots and Systems*. IEEE, 2014, pp. 2126–2133.

[15] M. Sharifi, H. Talebi, and M. Shafiee, "Adaptive estimation of robot environmental force interacting with soft tissues," in *2015 3rd RSI International Conference on Robotics and Mechatronics (ICROM)*. IEEE, 2015, pp. 371–376.

[16] S. Abeywardena, Q. Yuan, A. Tzemanaki, E. Psomopoulou, L. Droukas, C. Melhuish, and S. Dogramadzi, "Estimation of tool-tissue forces in robot-assisted minimally invasive surgery using neural networks," *Frontiers in Robotics and AI*, vol. 6, p. 56, 2019. [Online]. Available: https://www.frontiersin.org/article/10.3389/frobt.2019.00056

[17] G. Peng, C. Yang, W. He, and C. L. P. Chen, "Force sensorless admittance control with neural learning for robots with actuator saturation," *IEEE Transactions on Industrial Electronics*, vol. 67, no. 4, pp. 3138–3148, 2020.

[18] A. Mendizabal, R. Sznitman, and S. Cotin, "Force classification during robotic interventions through simulation-trained neural networks," *International journal of computer assisted radiology and surgery*, vol. 14, no. 9, pp. 1601–1610, 2019.

[19] A. Marban, V. Srinivasan, W. Samek, J. Fernández, and A. Casals, "A recurrent convolutional neural network approach for sensorless force estimation in robotic surgery," *Biomedical Signal Processing and Control*, vol. 50, pp. 134–150, 2019.

[20] A. Dong, Z. Du, and Z. Yan, "A sensorless interaction forces estimator for bilateral teleoperation system based on online sparse gaussian process regression," *Mechanism and Machine Theory*, vol. 143, p. 103620, 2020.

[21] F. Alonge, A. Bruno, and F. D'ippolito, "Interaction control of robotic manipulators without force measurement," in *2010 IEEE International Symposium on Industrial Electronics*. IEEE, 2010, pp. 3245–3250.

[22] S.-J. Huang, Y.-C. Liu, and S.-H. Hsiang, "Robotic end-effector impedance control without expensive torque/force sensor," *International Journal of Mechanical, Aerospace, Industrial, Mechatronic and Manufacturing Engineering*, vol. 7, no. 7, pp. 1446–1453, 2013.

[23] M. P. Polverini, A. M. Zanchettin, S. Castello, and P. Rocco, "Sensorless and constraint based peg-in-hole task execution with a dual-arm robot," in *2016 IEEE International Conference on Robotics and Automation (ICRA)*. IEEE, 2016, pp. 415–420.

[24] F. Zhou, B. Dong, and Y. Li, "Torque sensorless force/position decentralized control for constrained reconfigurable manipulator with harmonic drive transmission," *International Journal of Control, Automation and Systems*, vol. 15, no. 5, pp. 2364–2375, 2017.

[25] T. T. Phuong, K. Ohishi, and Y. Yokokura, "Fine sensorless force control realization based on dither periodic component elimination kalman filter and wide band disturbance observer," *IEEE Transactions on Industrial Electronics*, vol. 67, no. 1, pp. 757–767, 2018.

[26] H. Nakamura, K. Ohishi, Y. Yokokura, N. Kamiya, T. Miyazaki, and A. Tsukamoto, "Force sensorless fine force control based on notch-type friction-free disturbance observers," *IEEJ Journal of Industry Applications*, vol. 7, no. 2, pp. 117–126, 2018.

[27] N. Hogan, "On the stability of manipulators performing contact tasks," *IEEE Journal on Robotics and Automation*, vol. 4, no. 6, pp. 677–686, 1988.

[28] L. Roveda, N. Iannacci, and L. M. Tosatti, "Discrete-time formulation for optimal impact control in interaction tasks," *Journal of Intelligent & Robotic Systems*, vol. 90, no. 3-4, pp. 407–417, 2018.

[29] S. A. M. Dehghan, M. Danesh, and F. Sheikholeslam, "Adaptive hybrid force/position control of robot manipulators using an adaptive force estimator in the presence of parametric uncertainty," *Advanced Robotics*, vol. 29, no. 4, pp. 209–223, 2015.

[30] L. Roveda, F. Vicentini, and L. M. Tosatti, "Deformation-tracking impedance control in interaction with uncertain environments," in *2013 IEEE/RSJ International Conference on Intelligent Robots and Systems*. IEEE, 2013, pp. 1992–1997.

[31] B. Siciliano and L. Villani, *Robot Force Control*, 1st ed. Norwell, MA, USA: Kluwer Academic Publishers, 2000.

[32] P. R. Chang and C. G. Lee, "Residue arithmetic vlsi array architecture for manipulator pseudo-inverse jacobian computation," in *Proceedings. 1988 IEEE International Conference on Robotics and Automation*. IEEE, 1988, pp. 297–302.

[33] N. Pedrocchi, E. Villagrossi, F. Vicentini, and L. Molinari Tosatti, "On robot dynamic model identification through sub-workspace evolved trajectories for optimal torque estimation," in *Intelligent Robots and Systems (IROS), 2013 IEEE/RSJ International Conference on*. IEEE, 2013, pp. 2370–2376.

[34] S. Jung, T. C. Hsia, and R. G. Bonitz, "Force tracking impedance control for robot manipulators with an unknown environment: theory, simulation, and experiment," *The International Journal of Robotics Research*, vol. 20, no. 9, pp. 765–774, 2001.

[35] R. E. Kalman *et al.*, "Contributions to the theory of optimal control," *Bol. soc. mat. mexicana*, vol. 5, no. 2, pp. 102–119, 1960.

[36] C. Gaz, M. Cognetti, A. Oliva, P. R. Giordano, and A. De Luca, "Dynamic identification of the franka emika panda robot with retrieval of feasible parameters using penalty-based optimization," *IEEE Robotics and Automation Letters*, vol. 4, no. 4, pp. 4147–4154, 2019.

[37] L. Roveda, "Adaptive interaction controller for compliant robot base applications," *IEEE Access*, vol. 7, pp. 6553–6561, 2018.

[38] L. Roveda, N. Castaman, P. Franceschi, S. Ghidoni, and N. Pedrocchi, "A control framework definition to overcome position/interaction dynamics uncertainties in force-controlled tasks," in *2020 IEEE International Conference on Robotics and Automation (ICRA)*. IEEE, 2020, pp. 6819–6825.

[39] L. Roveda, N. Iannacci, F. Vicentini, N. Pedrocchi, F. Braghin, and L. M. Tosatti, "Optimal impedance force-tracking control design with impact formulation for interaction tasks," *IEEE Robotics and Automation Letters*, vol. 1, no. 1, pp. 130–136, 2015.

[40] S. A. Krasnova, V. A. Utkin, and Y. V. Mikheev, "Cascade design of state observers," *Automation and Remote Control*, vol. 62, no. 2, pp. 207–226, 2001.

[41] Z. Lendek, R. Babuska, and B. De Schutter, "Stability of cascaded fuzzy systems and observers," *IEEE Transactions on Fuzzy Systems*, vol. 17, no. 3, pp. 641–653, 2008.

[42] H. K. Khalil, "Cascade high-gain observers in output feedback control," *Automatica*, vol. 80, pp. 110–118, 2017.